Del Genio A. D. (2013) Physical processes controlling Earth's climate. In *Comparative Climatology of Terrestrial Planets* (S. J. Mackwell et al., eds.), pp. 3–18. Univ. of Arizona, Tucson, DOI: 10.2458/azu_uapress_9780816530595-ch001.

Physical Processes Controlling Earth's Climate

Anthony D. Del Genio
NASA Goddard Institute for Space Studies

As background for consideration of the climates of the other terrestrial planets in our solar system and the potential habitability of rocky exoplanets, we discuss the basic physics that controls the Earth's present climate, with particular emphasis on the energy and water cycles. We define several dimensionless parameters relevant to characterizing a planet's general circulation, climate, and hydrological cycle. We also consider issues associated with the use of past climate variations as indicators of future anthropogenically forced climate change, and recent advances in understanding projections of future climate that might have implications for Earth-like exoplanets.

1. INTRODUCTION

The amazing diversity of atmospheric behavior seen in our own solar system represents a challenge to our fundamental understanding of atmospheric physics. The weather and climate of Earth, explored extensively during the past century, provide an invaluable basis for understanding this diversity. Yet Earth's atmosphere occupies only one part of the parameter space of factors that can affect weather and climate. The extent to which our terrestrial assumptions carry over to other planets must continually be evaluated. A planetary perspective on Earth can help us decide which features that we take for granted are unique to our planet and which it has in common with subsets of other planets. The rapidly growing list of discovered exoplanets, and the need to assess which of these might lie in the habitable zone (see Domagal-Goldman and Segura, this volume), stretches our assumed understanding of Earth. Furthermore, increasing evidence of conditions during Earth's own past, as well as the urgency to be able to predict important features of future anthropogenically forced climate change, has led to a resurgence in fundamental studies of Earth's present climate in recent years. The science of comparative planetary climatology is indeed coupled to questions of our own planet's past and future habitability (see Foreword to this volume).

Although there is still much we do not understand about our own climate system, orders of magnitude more theoretical, observational, and modeling effort has been devoted to our planet than any other. Thus, for solar system or exoplanet researchers reading this book, we hope that starting with a discussion of Earth will provide a useful, even necessary, foundation for thinking about conditions on other planets. For terrestrial scientists, we hope that the planetary perspective of Earth presented in this chapter will stimulate thinking about the features that make Earth unique in our solar system. The time has never been riper for such thinking, since the advent of general circulation models (GCMs) (see Dowling, this volume) run on high-performance computing platforms now makes it possible to ask almost any imaginable "What if . . .?" question about Earth and the physics that control its climate. This chapter assumes a knowledge of basic atmospheric science; derivations and further discussion of many of the principles presented here can be found in textbooks such as *Houghton* (2002) and *Wallace and Hobbs* (2006).

2. THE ENERGY AND WATER CYCLES

New estimates of the solar irradiance of Earth (*Kopp and Lean,* 2011) indicate a value S_o = 1360.8 W/m^2 at solar minimum, considerably lower than previous estimates (see Harder and Woods, this volume). This so-called solar constant actually fluctuates by ~0.1 W/m^2 over the 11-year solar cycle, an inconsequential variation for Earth's climate. Averaged over the Earth, the absorbed shortwave (SW) flux equals the emitted longwave (LW) flux in equilibrium (see Covey et al., this volume):

$$\frac{S_o(1-A)}{4d^2} = \sigma T_e^4 \qquad (1)$$

where A = 0.293 is the planetary albedo (*Loeb et al.,* 2009), d the planet-Sun distance in astronomical units (=1 for Earth), σ the Stefan-Boltzmann constant, and T_e the effective temperature of a blackbody that would produce the observed LW flux. Actually, Earth is currently out of equilibrium by ~0.6 W/m^2 due to anthropogenic emissions of greenhouse gases and other climate forcings (*Lyman et al.,* 2010).

Figure 1 shows the contributions to the global energy balance at the top-of-atmosphere (TOA), within the atmospheric column, and at the surface (*Stephens et al.,* 2012). Clouds account for almost half of Earth's planetary albedo; the other half is made up of almost equal contributions from

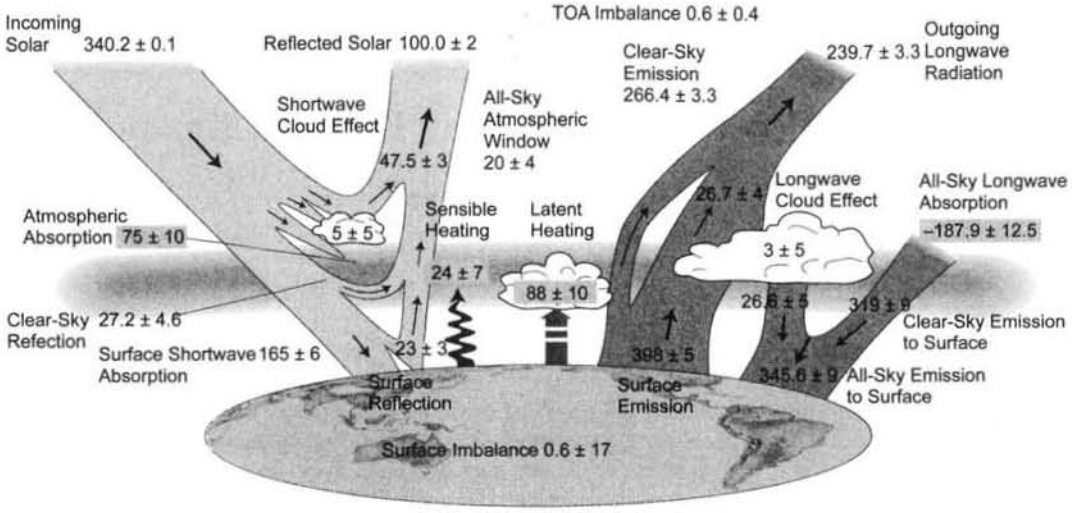

Fig. 1. See Plate 1 for color version. Estimate of the components of the current annual mean energy balance of Earth at TOA (upper row), within the atmosphere (middle row), and at the surface (bottom row). SW fluxes are in yellow, LW fluxes in magenta, and surface turbulent fluxes in red and violet. From *Stephens et al.* (2012). ©Copyright Nature Publishing Group; reprinted with permission.

the clear atmosphere (aerosol scattering and gaseous Rayleigh scattering) and the surface. The outgoing LW flux to space comes almost entirely from the atmosphere, with only an 8% contribution from the surface that escapes through the atmospheric thermal infrared window. Even in clear skies, the surface only contributes ~25% of the emission to space because of the LW opacity of greenhouse gases (*Costa and Shine,* 2012).

Earth's atmosphere is fairly transparent to our Sun's radiation, which peaks in the visible; ~22% is absorbed within the atmosphere, primarily due to O_2 and O_3 in the ultraviolet, H_2O in the near-infrared, and absorbing aerosols in the visible. The SW flux that reaches the surface is primarily (~88%) absorbed. The surface energy budget is balanced largely by upward surface turbulent latent and heat fluxes and partly by the net (up–down) LW flux (see Showman et al., this volume). The LW contribution is secondary because atmospheric absorbers induce a downward LW flux that offsets much of the upward emission from the surface.

T_e in equation (1) = 255 K, 33 K colder than Earth's surface temperature T_s = 288 K. The difference is a measure of Earth's greenhouse effect (see Covey et al., this volume) due to LW absorbers. Water vapor accounts for ~50% of the greenhouse effect, followed by clouds (~25%), CO_2 (~19%), and other absorbing gases and particulates (~7%) (*Schmidt et al.,* 2010). These relative contributions obscure the fact that CO_2 is actually the primary driver of Earth's climate, since water vapor is controlled (largely via the Clausius-Clapeyron equation of thermodynamics) by the heating due to CO_2 and other noncondensable greenhouse gases (*Lacis et al.,* 2010). Figure 2, for example, shows that when CO_2 and other noncondensable greenhouse gases are removed from an Earth GCM, the planet cools by ~35°C and the water vapor content is reduced by 90%. On Titan (see Griffith et al., this volume), the noncondensable absorber H_2 exerts a similar control on the climate by regulating the concentration of the condensable gas CH_4 (*McKay et al.,* 1991).

Figure 3 shows the geographic distribution of the TOA absorbed SW and outgoing LW flux in clear skies,

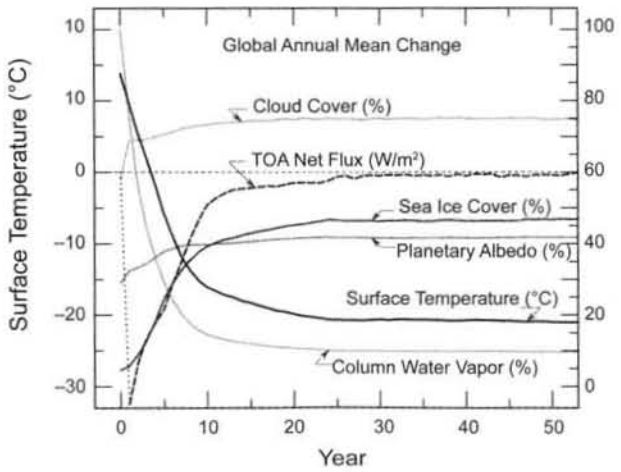

Fig. 2. Temporal evolution of surface temperature, column water vapor, TOA net radiative flux, cloud cover, sea ice cover, and planetary albedo in a GCM coupled to a 250-m Q-flux ocean after the concentrations of CO_2 and other noncondensing greenhouse gases were set to zero. From *Lacis et al.* (2010). ©Copyright American Association for the Advancement of Science; reprinted with permission.

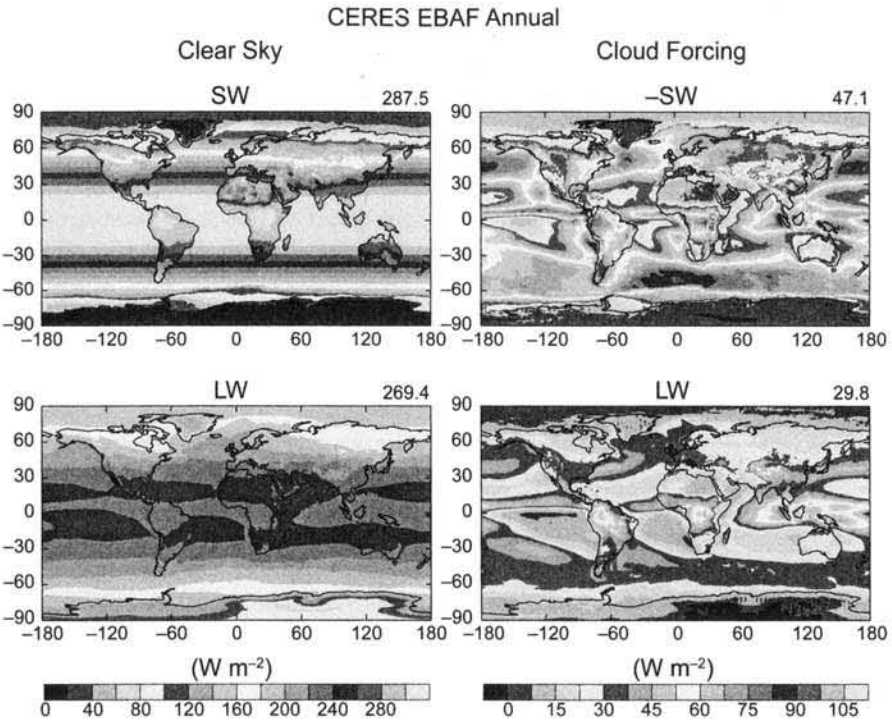

Fig. 3. See Plate 2 for color version. TOA Earth SW (upper panels) and LW (lower panels) annual mean clear-sky fluxes (left panels) and cloud forcing (right panels) derived from the NASA Clouds and the Earth's Radiant Energy System Energy Balanced and Filled (CERES EBAF) data product. The global mean values are given in the upper right corner of each panel. The SW cloud forcing has been multiplied by –1 for display purposes. Figure courtesy of J. Jonas.

and the difference between that and the total fluxes in all conditions, known as the "cloud forcing" or "cloud radiative effect" (*Loeb et al.,* 2009). The clear sky SW flux is dominated by the solar zenith angle variation with latitude, but departures from the zonal mean at each latitude reveal radiatively important details of Earth's surface: minima over bright ice-covered Greenland and Antarctica and to a lesser extent over the Arctic and Antarctic sea ice packs, maxima over the dark oceans, and intermediate values over other land surfaces.

The other fluxes are regulated primarily by the atmosphere and are thus indicators of the general circulation. Earth's "tropical" and "extratropical" dynamical regimes are determined by its radius, rotation period, and thermodynamic structure (see Showman et al., this volume). Low-level moisture convergence and deep convection in the rising branch of the Hadley cell maximize the greenhouse effect near the equator and produce a minimum in clear sky LW flux to space there relative to the flux maxima in the surrounding subtropical dry subsidence regions. Otherwise the clear sky flux reflects primarily the decrease in temperature and water vapor with latitude. Longwave cloud forcing (which is positive because clouds reduce LW emission to space and thus warm the planet) peaks coincide with the tropical locations of deep convection; secondary maxima exist in the extratropical storm tracks. Shortwave cloud forcing (which is negative because clouds are brighter than most of Earth's surface and thus cool the planet) also is large in magnitude in these regions. Other SW cloud forcing maxima exist off the west coasts of the continents but with no corresponding LW signal. These are locations of low-level marine stratocumulus decks whose tops are below the clear sky emission to space level. Globally averaged, SW cooling by clouds exceeds LW warming by ~17 W/m^2, i.e., the net effect of clouds is to cool the current climate.

Aerosols (Fig. 4) have three qualitatively different effects on the climate: (1) *Direct effects* due to their interaction with (mostly SW) radiation (*Myhre,* 2009). Since most aerosol types (sulfates, nitrates, sea salt, and organic carbon) are bright, they cool Earth. However, black carbon and mineral dust absorb SW radiation; this cools the surface by preventing sunlight from reaching it but warms the atmosphere and the planet as a whole. This is analogous to the "anti-greenhouse" effect of absorbing hydrocarbon hazes on Titan (*McKay et al.,* 1991; Griffith et al., this volume), but with a smaller magnitude. (2) *Indirect effects* due to the interaction of aerosols with clouds (*McComiskey and Feingold,* 2012). Aerosols act as cloud condensation nuclei and affect the number concentration and size of cloud droplets. With an increase in aerosols, the available water is shared among

more but smaller droplets, increasing their area/volume ratio and thus making the cloud more reflective. Smaller cloud droplets may also affect the microphysics and dynamics of clouds, but the magnitude of this effect is quite uncertain. (3) *Semi-direct effects* due to the influence of warming by absorbing aerosols on the atmospheric thermodynamic structure (*Koch and Del Genio,* 2010). For example, marine stratocumulus clouds that occur under strong inversions may become more widespread if an absorbing aerosol advected from an adjacent continent increases the inversion strength.

The geographic distribution of aerosols (*Bauer et al.,* 2008) is determined by natural and anthropogenic sources, tropospheric chemical reactions, wet and dry deposition, and advection by the general circulation. Sulfate and nitrate are largely of anthropogenic origin and are concentrated near and downwind of industrial, transportation, and agricultural sources. Organic and black carbon are most prevalent in regions of biomass burning, but also have important industrial and transportation sources. Mineral dust is mostly natural in origin, the largest source region being the Sahara and Arabian deserts. Sea salt is produced mainly in oceanic regions of strong surface winds such as the extratropical storm tracks.

Although the TOA-absorbed SW and outgoing LW radiative fluxes must balance globally for the climate to be in equilibrium, this is not true locally. In fact, there is a latitudinally varying imbalance of net radiative heating on Earth (Fig. 5): The tropics receives more sunlight than the heat it emits to space, while higher latitudes emit more than they absorb. In equilibrium this must be offset by the transport of heat from low to high latitudes. This is the fundamental driver of the circulations of the atmosphere and ocean (*Trenberth and Caron,* 2001). The atmospheric component of heat transport is accomplished primarily by the Hadley circulation in the tropics and by synoptic-scale eddies created by baroclinic instability in the extratropics (see Showman et al., this volume) and dominates at high latitudes. The ocean circulation contribution to transport dominates at low latitudes (Fig. 6).

The ocean circulation has two fundamental components: a surface circulation in the top ~100 m driven by the frictional interaction with atmospheric surface winds and the Coriolis force, and a thermohaline circulation driven by density gradients due to temperature and salinity differences. The surface winds created by Earth's three-cell mean meridional circulation produce tropical easterly and extratropical westerly ocean currents. At longitudinal continental boundaries, the easterlies are deflected poleward and the westerlies equatorward, forming roughly circular ocean gyres in each ocean basin and hemisphere. The gyres transport warm water poleward off the east coasts of the continents and cold water equatorward off the west coasts, effecting a net poleward heat transport (*Klinger and Marotzke,* 2000). The wind-driven transport may be an important factor in limiting sea ice expansion to the tropics in "snowball Earth" scenarios (*Poulsen and Jacob,* 2004; *Rose and Marshall,* 2009). At high latitudes, dense (cold and/or salty) water sinks to the ocean bottom and slowly circulates to lower latitudes. High-salinity water is produced by net evaporation (i.e., in excess of precipitation) and the formation of sea ice, which cannot easily accommodate salt and thus produces salty ocean water where it occurs. The

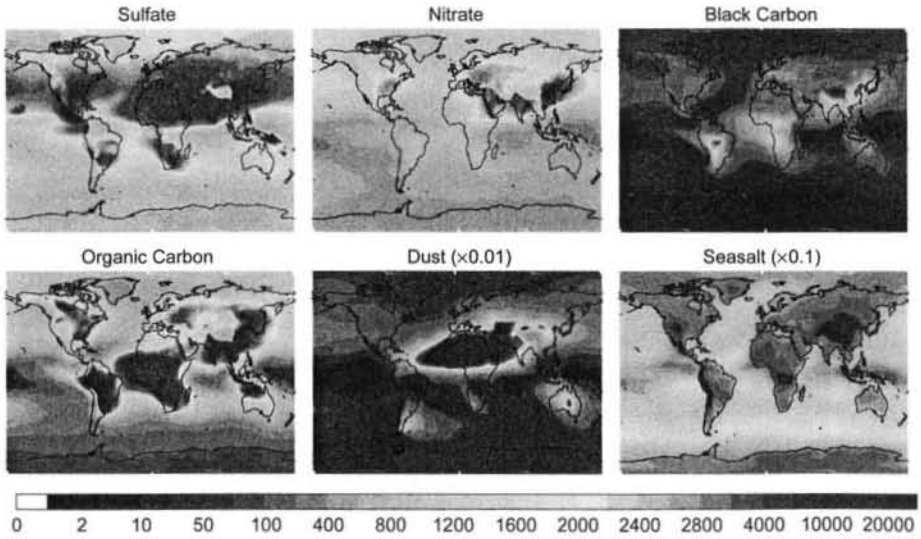

Fig. 4. See Plate 3 for color version. Annual mean column mass concentrations (μg/m^2) of the six major Earth aerosol types, calculated from the MATRIX model in the Goddard Institute for Space Studies GCM (*Bauer et al.,* 2008). The dust and sea salt concentrations have been multiplied by factors of 0.01 and 0.1, respectively. Figure courtesy of S. Bauer.

"deep water" that forms at high latitudes must be replaced by warm surface water transported from lower latitudes, adding to the poleward heat transport (*Broecker,* 1991). The removal of dense surface water to the deep ocean takes it out of thermal contact with the atmosphere until it returns to the surface at low latitudes much later. This implies that the effects of changes in greenhouse gas concentrations will not fully be reflected in surface temperatures for centuries, perhaps even a millennium or more (*Hansen et al.,* 1985).

Stone (1978a) argued that the total meridional heat transport is controlled by external parameters (solar constant, planet size, and obliquity) and the planetary albedo, and thus that the details of partitioning between atmosphere and ocean are unimportant. This would be good news for exoplanet science, since nothing is known about possible oceans on exoplanets. However, *Enderton and Marshall* (2009) show that in an idealized "aquaplanet" Earth GCM, Stone's conclusion is valid only for warm, ice-free climates. *Ferreira et al.* (2011) find that multiple equilibria, from ice-free to ice-covered ("snowball") states are possible in such models. Figure 7 compares two versions of an Earth atmospheric GCM coupled to a mixed-layer ocean with specified ocean heat transports. One has transports calculated to produce observed sea surface temperatures — a "Q-flux" model (*Hansen et al.,* 1984) — and another has ocean heat transports turned off. The atmosphere has clearly not compensated for the absence of ocean heat transport, leading to much more extensive sea ice coverage and a clearly different climate for the same external forcing.

Vertical heat transport is just as important in determining the Earth's climate. The simplest assumption for the vertical thermodynamic structure is to assume that it is in radiative equilibrium, i.e., the temperature profile is such that the divergence of the radiative flux is zero at all levels. Simple pedagogical models that assume an atmosphere transparent to SW radiation but with a nonzero gray (i.e., wavelength-independent) LW optical thickness τ^* predict a surface temperature given by

$$T_s^4 = \left(1 + c\tau^*\right) T_e^4 \tag{2a}$$

where c is a constant that depends on the details of the model. This equation shows that a planet with an atmosphere containing greenhouse gases has a surface temperature that exceeds its effective temperature, to a greater degree as the atmosphere becomes optically thicker. (An exception to this rule is a planet such as Mars with large day-night T_s contrasts; see Rafkin et al. and Covey et al., this volume). Equation (2a) can be modified to incorporate atmospheric SW absorption due, e.g., to an ozone layer or an absorbing haze (*McKay et al.,* 1999), giving

$$\sigma T_s^4 = \left(1-\gamma\right) F_s \left(1 + c\tau^*\right) + \frac{\gamma F_s}{2} \tag{2b}$$

where $F_s = S_o(1-A)/4d^2$ is the SW flux absorbed by the planet and γ is the fraction of this flux that is absorbed within the atmosphere (see Covey et al., this volume). Equations (2a) and (2b) are not quantitatively accurate but capture the basic physics of how the atmosphere radiatively modulates surface temperature.

Models that lead to equation (2a) inherently produce a surface-atmosphere temperature discontinuity because the surface absorbs all the incident SW radiation. Furthermore, the T_s they predict considerably exceeds the observed T_s for realistic τ^*. More sophisticated one-dimensional radiative equilibrium models also indicate that the lower troposphere lapse rate of Earth in radiative equilibrium is superadiabatic (*Manabe and Strickler,* 1964). Thus an adjustment, either

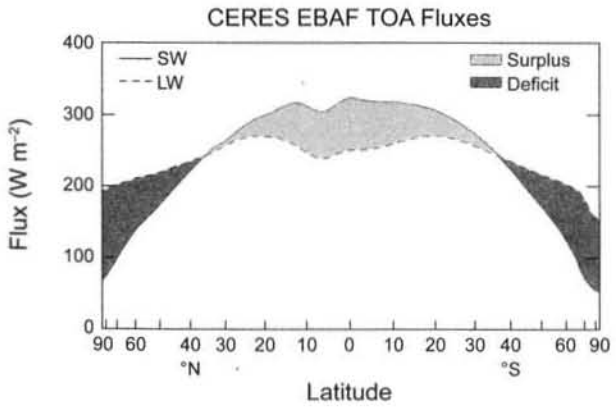

Fig. 5. Zonal and annual mean Earth TOA absorbed SW (solid) and outgoing LW (dashed) radiative fluxes from CERES EBAF data. The light shaded area shows latitudes at which the net radiative energy input to the Earth system is positive, the darker area where it is negative. Figure courtesy of J. Jonas.

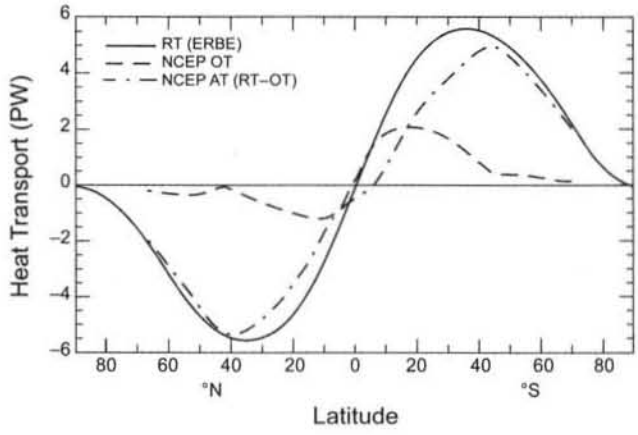

Fig. 6. Latitudinal profiles of the annual mean Earth total energy transport (solid) required by the observed latitudinal profiles of TOA radiative fluxes, and its estimated partitioning into ocean (OT, dashed) and atmosphere (AT, dash-dot) components. From *Trenberth and Caron* (2001).

to a specified threshold lapse rate (dry or moist adiabatic) or determined by a more detailed model of convection, is applied to limit lapse rates and produces a realistic T_s and temperature profile. The implied upward transport of heat by convection reduces the sensitivity of T_s to changes in atmospheric composition or insolation.

Observations indicate that Earth's tropical lapse rate in the free troposphere is close to moist adiabatic up to ~400 hPa (*Zelinka and Hartmann,* 2011), indicating that moist convection is the controlling process up to that level (Fig. 8). This is possible because over the warm tropical oceans, the boundary layer is sufficiently humid for moist convection to occur frequently enough to adjust conditionally unstable lapse rates to near-neutral stability. This is not the case over the cooler tropical ocean regions, but the weak tropical Coriolis force allows advection to adjust the free troposphere lapse rate there to a value close to that in the warmer ocean regions (see Showman et al., this volume). Over tropical land, where moisture is not always available and the surface temperature responds more quickly to solar heating, more unstable lapse rates can sometimes occur; consequently, continental convective updraft speeds are stronger than those over ocean (*Zipser and Lutz,* 1994). Above the 400-hPa level, convective influence is more sporadic because entrainment of dry air often limits convection penetration depth (*Del Genio,* 2012).

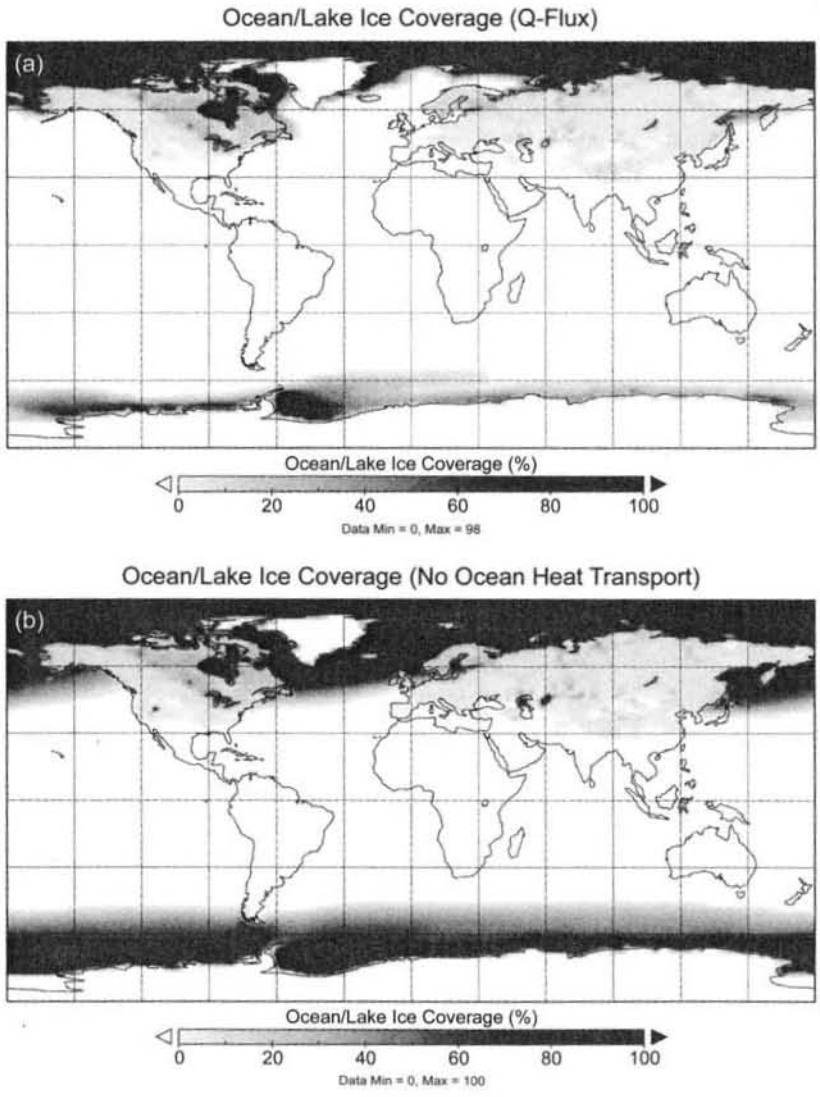

Fig. 7. December-January-February sea ice and lake ice coverage simulated by the Goddard Institute for Space Studies atmospheric GCM coupled to a mixed layer ocean with specified ocean heat transports. **(a)** Ocean heat transports are specified to reproduce observed SSTs ("Q-flux" model). **(b)** Ocean heat transports are turned off, so SSTs are determined solely by the surface flux the atmosphere provides to the ocean. Figures courtesy of M. Way.

Poleward of ~30° latitude, the tropospheric lapse rate is more stable than predicted by the moist adiabatic lapse rate. Surprisingly, extratropical static stability (proportional to the difference between the dry adiabatic and actual lapse rate) is not understood as well as tropical static stability despite our firmer understanding of extratropical quasi-geostrophic dynamics. *Stone* (1978b) suggested that the lapse rate is set by the requirement that dry baroclinic eddies associated with latitudinal temperature gradients adjust the atmosphere to a baroclinically neutral state. More recent work indicates that the extratropical lapse rate is affected by synoptic transports by both baroclinic eddies and moist convection (*Frierson,* 2008), but there is not universal agreement on the details. An effective static stability that is based on the moist adiabat but also accounts for dry downwelling circulations and meridional temperature gradients appears to hold promise (*O'Gorman,* 2011).

Equilibrium of the water cycle requires that on climate timescales, global mean precipitation P must balance global mean evaporation E. Just as for the energy cycle, though, the local water cycle is not balanced between sources and sinks (*Trenberth et al.,* 2007). Instead, the surface water balance E-P reflects the general circulation, with P > E in the moist equatorial rising branch of the Hadley cell and the extratropical storm tracks, and E > P in the dry subtropical descending branches of the Hadley cell (Fig. 9). The general circulation offsets these imbalances, with net moisture convergence into the equatorial region (hence the name Intertropical Convergence Zone) and net moisture divergence from the subtropics. Thus a significant amount of tropical precipitation does not originate from locally evaporated water.

The existence of tropical and extratropical dynamical regimes (see Showman et al., this volume) on Earth, plus the presence of preferred upwelling and downwelling regions in each, creates four basic climate or habitability zones: (1) *equatorial*, characterized by weak stratification, high humidity, and regular though intermittent strong precipitation; (2) *subtropical*, with weak stratification (except for low-level inversions) but low humidity, and therefore weak precipitation; (3) *midlatitude*, with stronger stratification and high humidity, and therefore regular slowly varying moderate precipitation; and (4) *polar*, characterized by strong stratification and low humidity, and thus weak precipitation. Life exists in each of these zones, but the more extreme conditions and life forms of the subtropical and polar desert regimes are less likely to be detected from space. The more abundant life that thrives in the more heavily precipitating equatorial and midlatitude regimes is more likely to provide an exoplanet biosignature.

A similar water cycle imbalance applies to different surface types. The oceans evaporate ~10% more water than they precipitate, and vice versa for land (Fig. 10). Thus there is a net atmospheric transport of water from ocean to land, implying that in some regions, continental precipitation is provided more by remote ocean sources than by local evapotranspiration. Water returns to the ocean via surface runoff and subsurface groundwater flow.

At TOA, the energy cycle is purely radiative, as given by equation (1). However, at the surface and within the atmosphere, the energy cycle (Fig. 1) and water cycle (Fig. 10) are directly coupled. At the surface, the turbulent fluxes that balance most of the absorbed sunlight (Fig. 1) are

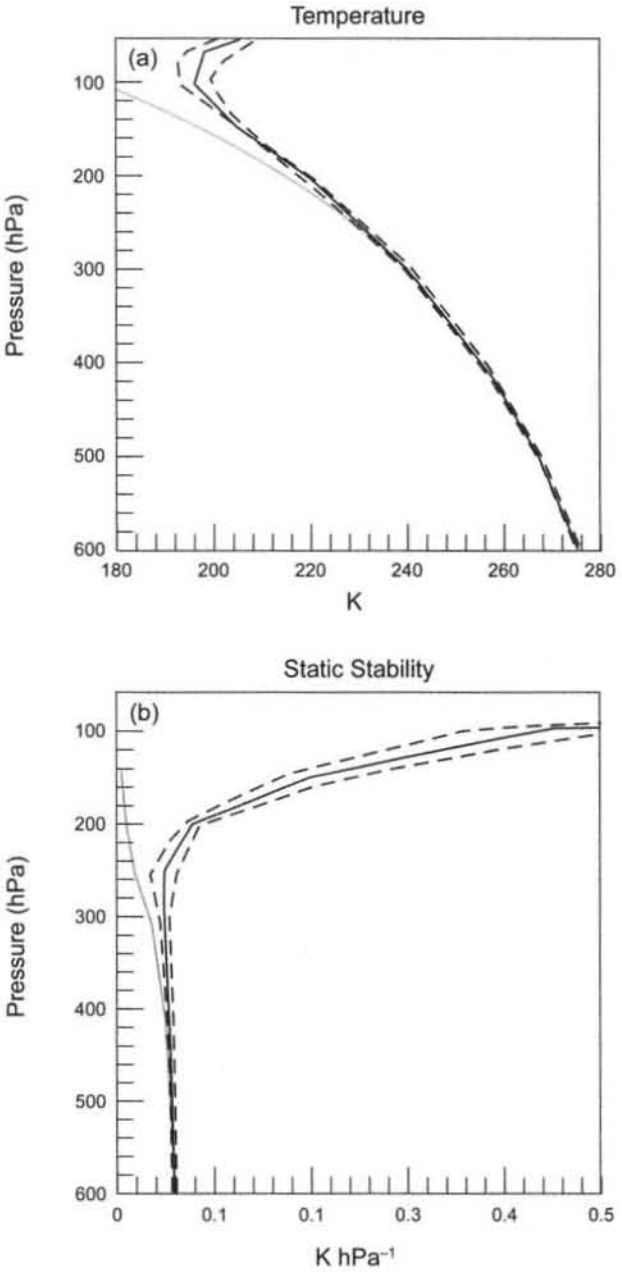

Fig. 8. Observed tropical mean vertical profiles of **(a)** temperature and **(b)** static stability for Earth's middle and upper troposphere (solid black curves). The dashed black curves represent the 2σ range of variability of the tropical means. The solid gray curves are the temperature and static stability profiles of a moist adiabat with an 850-hPa temperature equal to that observed. Adapted from *Zelinka and Hartmann* (2011). ©Copyright American Geophysical Union; reprinted with permission.

dominated by the latent heat flux (evaporation) over ocean; i.e., the Bowen ratio of sensible to latent heat flux is small, while over land the ratio varies considerably according to the soil moisture. This, in addition to the greater thermal inertia of the ocean, causes surface temperatures to respond much more strongly to perturbations over land than over ocean. Within the atmosphere, the net radiative cooling of the column (outgoing LW to space + downward surface LW–upward surface LW–SW absorption) is balanced by turbulent fluxes from the surface, mostly by the latent heat flux when water vapor condenses and precipitates (see Showman et al., this volume). Thus, precipitation in GCMs depends not only directly on the physical processes that produce precipitation (e.g., moist convection), but indirectly on phenomena whose direct influences are only radiative (e.g., the areal coverage of nonprecipitating stratocumulus clouds).

3. DIMENSIONLESS NUMBERS AS CLIMATE INDICATORS

To translate this knowledge to other planets and anticipate similarities and differences, we need to understand why particular processes control particular aspects of the climate. In general, when multiple processes occur, the fastest process dominates, and so it is instructive to define characteristic time or length scales for different processes and form appropriate dimensionless ratios to assess their importance.

This approach is well known in atmospheric dynamics, where quantities such as the Rossby number (see Showman et al., this volume), the ratio of the advective to Coriolis forces, differentiate the tropical from the extratropical dynamical regime. Another useful dimensionless number is the Richardson number $\mathrm{Ri} = [\mathrm{N}/(\mathrm{du}/\mathrm{dz})]^2$, where N, the Brunt-Väisälä frequency, describes the vertical stratification of the atmosphere, and the vertical wind shear dU/dz for large-scale gradient wind-balanced flows is related to the meridional temperature gradient via the thermal wind equation (see Showman et al., this volume). *Allison et al.* (1995) showed that the ratio of the potential temperature (the temperature of a parcel moved adiabatically to a given reference pressure) contrasts $\Delta_V\theta$ and $\Delta_H\theta$ over the vertical and horizontal scales of the flow (the slope of the isentropes) is

$$\frac{\Delta_V\theta}{\Delta_H\theta} \sim \frac{\mathrm{Ri}}{\mathrm{D}^*}\left(1+\frac{1}{\mathrm{Ro}}\right)^{-1} \tag{3}$$

where D^* is the depth of the flow in scale heights, $\mathrm{Ro} = \mathrm{U}/\Omega a$ is a global Rossby number based on the planet angular rotation frequency Ω and radius a, and Ri is expressed in log pressure coordinates. Figure 11 shows that Ri and Ro separate the planets in our solar system into three dynamical regimes. The slowly rotating planets Venus (Bullock and Grinspoon, this volume) and Titan (Griffith et al., this volume) have $\Delta\theta_v \gg \Delta\theta_h$, due to stabilizing upper level aerosol

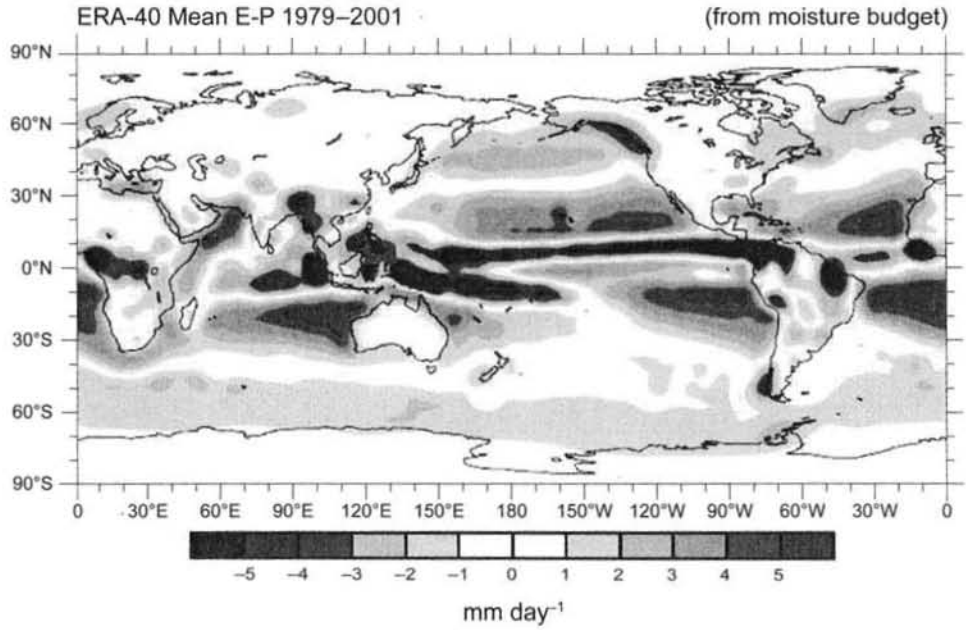

Fig. 9. See Plate 4 for color version. The annual mean Earth surface water budget E-P calculated from monthly means of the vertically integrated moisture budget of the atmosphere in the European Centre for Medium Range Weather Forecasts 40-year reanalysis (ERA-40). From *Trenberth et al.* (2007). ©Copyright 2007 American Meteorological Society; reprinted with permission.

haze decks and the broad Hadley cells that accompany slow rotation and efficiently transport heat poleward (see also Showman et al., this volume). On the jovian planets, $\Delta\theta_v \ll \Delta\theta_h$ because of their internal heat sources and convective interiors that effectively transport heat upward (*Gierasch,* 1976). Only Earth and Mars (Rafkin et al., this volume) share the intermediate regime $\Delta\theta_v \sim \Delta\theta_h$, for which both meridional and vertical transport matter. No known terrestrial planets occupy the high Ro, low Ri corner of Fig. 11, but GCMs suggest that a slowly rotating Earth with few clouds or hazes, significant surface SW absorption, and thus a convective troposphere might reside in this part of parameter space (*Del Genio et al.,* 1993).

To organize our thinking about the importance of moist processes and the combined temperature and water conditions that are most conducive to supporting life, it is useful to define several energy and water-related timescales that might be relevant to assessments of habitability:

1. The radiative time constant $t_{rad} = pc_pT/gF$ is the ratio of atmospheric heat content to the rate of radiative cooling to space F of a layer of depth one scale height. An analogous time constant with suitable values of the heat capacity for different thicknesses of fluid can be used to explain the timescales on which the ocean mixed layer, thermocline, and deep ocean respond to radiative perturbations at the surface.

2. The residence time of water $t_{res} = PW/P$, similarly defined as the ratio of the column water vapor content PW to the precipitation rate P, measures the vigor of the hydrologic cycle.

3. The dynamical timescales for synoptic scale weather variability ($t_{ds} = L/U$), where L is a typical length scale for synoptic flow; for planetary scale heat transport ($t_{dp} = a/V$), where V is a typical mean meridional wind speed; and for convective adjustment of the lapse rate ($t_{con} = H/W$), where H is the scale height and W a typical convective updraft speed, assess the importance of transports by different dynamical mechanisms.

4. External astronomical timescales such as the diurnal (t_{day}) and seasonal (t_{year}) timescales measure the importance of variations in solar/stellar forcing.

From these time constants a variety of potentially useful dimensionless numbers can be constructed. For example, numerical weather prediction models of Earth need not acknowledge the rising and setting of the Sun to predict the arrival of a low pressure center and rain in 24 hr because $t_{ds}/t_{rad} \ll 1$, but the general circulation and climate of Earth vary nonnegligibly with the seasons because t_{dp}/t_{year} and $t_{rad}/t_{year} \sim 1$. Seasonally varying temperatures lag seasonally varying insolation by a phase shift of $\tan^{-1}(2\pi t_{rad}/t_{year})$, and the amplitude of the seasonal cycle of temperature is t_{year}/t_{rad} when this ratio is small (*Conrath and Pirraglia,* 1983). Thus the impact of large orbital eccentricity on exoplanet habitability will be more muted in a thicker atmosphere.

A useful measure of the role of moist processes in a planet's climate might be given by the ratio t_{res}/t_{rad}, with a small value being diagnostic of a vigorous hydrologic cycle (presumably of interest for habitability) and its importance to the circulation and surface energy balance. For Earth

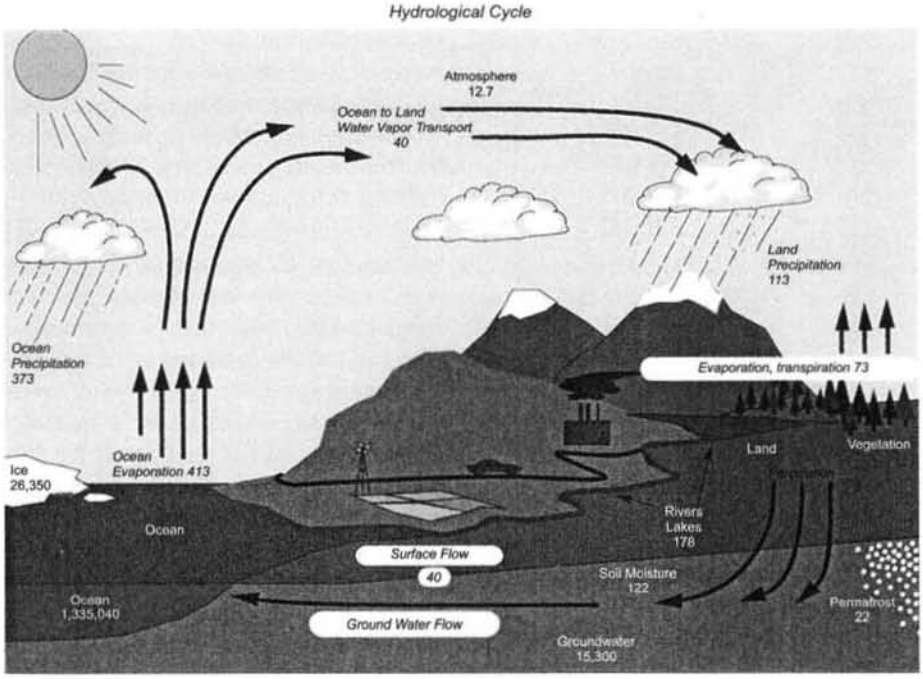

Fig. 10. See Plate 5 for color version. Global annual mean components of Earth's hydrological cycle. Storage amounts in the reservoirs are given in roman font, and flows/exchanges between reservoirs in italics (units are 1000 km^3). From *Trenberth et al.* (2007). ©Copyright 2007 American Meteorological Society; reprinted with permission.

(to date, a habitable planet) t_{res} ~ 8 d and t_{rad} ~ 2 months, giving t_{res}/t_{rad} ~ 0.1. For Titan, t_{rad} ~ 300 yr in the lower troposphere (*Strobel et al.,* 2009), while for methane, the condensable gas there, t_{res} ~ 75 yr (*Mitchell,* 2012). This gives t_{res}/t_{rad} ~ 0.25, consistent with its occasional observed storms and apparent control of its general circulation by moist processes (*Turtle et al.,* 2011). The long timescales for Titan are a consequence of its cold temperature, which would make it uninhabitable even if the condensable gas there was not methane. But their ratio nonetheless suggests a strong hydrologic cycle. The most habitable exoplanets might thus be defined not only by their global mean surface temperature, but also by small t_{res}/t_{rad}, and for those in highly eccentric orbits, modest spatial-temporal variability in temperature ($t_{rad}/t_{year} > 1$, $t_{dp}/t_{year} < 1$).

Dimensionless numbers can also correct misconceptions even about Earth's atmosphere. For example, one-dimensional models assume radiative-convective equilibrium, i.e., superadiabatic lapse rates are adjusted to a neutrally stable lapse rate. This is only valid if $t_{con}/t_{rad} \ll 1$, i.e., convection stabilizes the atmosphere much faster than radiation destabilizes it. This may not be the case if the condensable gas is present at too low a relative humidity (another dimensionless ratio) to trigger convection or to allow it to penetrate sufficiently deep to stabilize the thermal structure. "Quasi-equilibrium" theories that underlie many GCM cumulus parameterizations assume that $t_{con}/t_{ds} \ll 1$, i.e., moist convection is a "slave" to the large-scale dynamical forcing and quickly equilibrates to neutralize the large-scale state. Yet diurnal departures from quasi-equilibrium occur because t_{con}/t_{day} is not sufficiently small (*Jones and Randall,* 2011). Sometimes convection organizes into a mesoscale cluster with "memory," i.e., the current state depends on its prior evolution, lengthening t_{con} and invalidating $t_{con}/t_{ds} \ll 1$ (*Zimmer et al.,* 2011).

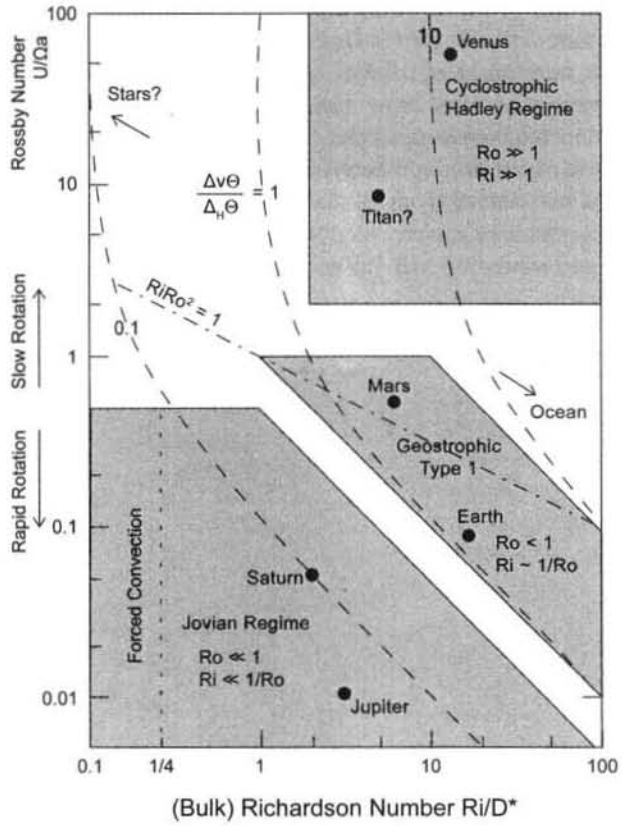

Fig. 11. Richardson-Rossby number diagram for defining atmospheric dynamical regimes of solar system planets. The three primary regimes (jovian, geostrophic, cyclostrophic/Hadley) are shaded. Dashed lines represent factor of 10 intervals in isentropic slope. The dash-dot line represents a value of the Burger number $B = RiRo^2 = 1$, which for the geostrophic regime indicates a characteristic length scale equal to the Rossby radius of deformation (see Showman et al., this volume). From *Allison et al.* (1995). ©Copyright American Geophysical Union; reprinted with permission.

4. LESSONS FROM TERRESTRIAL CLIMATE CHANGE

Most readers of this book will think of other planets when they hear the term "comparative climatology." However, Earth's own history, and its projected near-term future, are also exercises in comparative climatology. These have considerable relevance for issues such as the limits of the habitable zone for exoplanets. For in-depth analysis of specific climate change issues we refer the reader to the chapters in this volume by Covey et al. (greenhouse effect and feedbacks), Zent (orbital variability effects), Harder and Woods (solar variability effects), and Tian et al. (climate evolution). In this section we instead consider what we have and have not yet learned about Earth in particular, and climate change processes in general, from studying past and future climates.

The most relevant climate change topic for a planetary audience is the sensitivity of Earth's climate to external forcings. The only way for the *global* climate to change is via an imbalance between absorbed SW radiation (Q) and outgoing LW radiation (F). From equation (1), this can only be initiated by a change in solar (or stellar) luminosity, changing S_o; a forced change in planetary albedo A (due to a volcanic eruption, aerosol emissions, deforestation, etc.); or a change in greenhouse gas concentrations (which changes the LW opacity and thus moves the emission-to-space level to a different altitude, temporarily changing T_e). For the purpose of evaluating habitable zone limits for exoplanets, the same thing is accomplished by changing d in equation (1) (e.g., *Abe et al.,* 2011). Once a climate change is externally forced, internal feedbacks (see Covey et al., this volume) further alter A and T_e as the system tries to equilibrate. For a gradual climate perturbation such as anthropogenic emission of greenhouse gases, the most rapid response is a cooling of the stratosphere, which is approximately in radiative equilibrium, followed shortly by warming of the troposphere and land surface (*Hansen et al.,* 2005). Tropopause height and emission level rise, but since the troposphere has warmed, T_e at the new higher emission level is not very different

from that before the onset of the climate change. Thus, as mentioned in section 2, today's climate is only out of balance by ~0.6 W/m^2. The surface temperature warms as the deeper troposphere convectively adjusts on the longer timescales associated with the thermal inertia of the ocean and climate feedbacks (*Hansen et al.,* 1985).

Historically an idealized "equilibrium climate sensitivity" has been estimated in GCMs by instantaneously doubling the concentration of CO_2 ("2×CO_2") in an atmospheric GCM coupled to a Q-flux ocean. This decreases F because the more opaque atmosphere radiates to space from a higher colder altitude, causing an imbalance Q > F that causes the planet to warm. When the climate equilibrates and Q = F once again, the resulting surface temperature change ΔT_s is referred to as the equilibrium climate sensitivity. In the current generation of GCMs being run for the fifth Coupled Model Intercomparison Project (CMIP5), a different way of estimating climate sensitivity is being employed that uses a regression based on the transient climate change of a fully coupled atmosphere-ocean model, which sometimes gives a different result.

4.1. Is the Past Prologue?

Unlike numerical weather prediction models, whose short-term weather forecasts are evaluated every day, we have no simple way to define observational metrics that are useful as indicators of the fidelity of climate change projections. Such metrics have been proposed (e.g., *Reichler and Kim,* 2008) but tend to be based on available datasets rather than a consideration of the factors that matter most to climate change. Even TOA radiative fluxes, which are ultimately the source of climate change, are useless as climate change metrics when only their current climate mean state is utilized (*Pincus et al.,* 2008; *Collins et al.,* 2011; *Klocke et al.,* 2011). Most previous studies have used *static metrics* such as monthly geographical distributions of climate parameters, as opposed to *process-based metrics,* which measure how some important aspect of the climate changes with time or as a function of some independent controlling parameter.

One possible way to constrain climate sensitivity is to use the changes that have occurred in Earth's past. Earth has experienced multiple cold (glacial) and warm (interglacial) periods in its history, which in principle can provide useful information. Some of the more dramatic possible climate changes occurred in the distant past, e.g., the hypothesized (and debated) snowball Earth episodes of the Neoproterozoic Era (1000–542 Ma) (*Sohl and Chandler,* 2007; *Abbot et al.,* 2012), which are relevant to the issue of the outer edge of the habitable zone. The paleoclimatic evidence for such distant epochs, however, is sparse. More recent periods such as the mid-Holocene (6 ka) are better documented but involve small (<1°C) climate changes that make them less useful for insights into the future (*Hargreaves and Annan,* 2009).

The epoch with the best combination of extensive documentation and a large magnitude of climate change is the Last Glacial Maximum (LGM) (21 ka). It has often been assumed that the LGM, and earlier glacials and interglacials associated with the Milankovitch cycles of orbital variations (see Zent, this volume), can be used to infer the sensitivity of a future warmed climate. One problem with this assumption is that the LGM climate is less well known than is needed to provide a simple constraint. Early attempts to simulate the LGM with GCMs used prescribed sea surface temperature (SST) anomalies derived from ocean proxies by the CLIMAP Project (see *Rind,* 2008). The CLIMAP SSTs had some unusual features, such as a mid-Pacific *warming* signal and only a small tropical ocean cooling signal of ~1.5°C, despite 10°C cooling at high latitudes and significant cooling based on different proxies in tropical land areas. These results implied a fairly low climate sensitivity, and multiple GCMs could not reproduce them. More recent LGM reconstructions (*Waelbroeck et al.,* 2009) have used multiple proxies instead, finding larger tropical cooling that implies a higher climate sensitivity. Today's GCMs do not use the proxy data directly but rather run coupled atmosphere-ocean models and use the reconstructions for evaluation. Nonetheless, some glaring inconsistencies between the models and the data remain, calling the interpretation of the proxies into question (*Brady et al.,* 2013).

The second problem with the LGM as a proxy for future climate sensitivity is that GCMs provide conflicting results. *Crucifix* (2006) found that four GCMs that spanned almost the full range of ΔT_s uncertainty for a doubling of CO_2 concentration also simulated almost identical climate sensitivities to each other in response to LGM climate forcings (Fig. 12). The discrepancies were mainly attributed to cloud feedbacks that changed sign between the colder and warmer climates in some of the models. This should not be a surprise given the nonlinearity of the climate system. *Ye et al.* (1998), for example, showed that convective available potential energy, which affects moist convection, varies differently in response to +2 and –2°C SST changes, because in the warmer climate, the current balance between convective heating and radiative cooling just intensifies, while in the cooler climate, convection decreases dramatically, yielding to the large-scale dynamics as the process that balances radiative cooling to first order. *Hargreaves et al.* (2012) have suggested that LGM tropical cooling is a good indicator of equilibrium climate sensitivity based on a larger ensemble of GCMs, but this test has not yet been applied to future climate change predictions, and inferences drawn from it are still subject to uncertainties in the interpretation of the observational proxies.

The message is not that past climates are useless as constraints on future climate, but rather that continued thought must be given to how we can best use what we know about them to differentiate responses that are robust to the type of climate change examined from those that are sensitive to different types of climate change or to uncertainties in the observations themselves. *Schmidt et al.* (2013) propose several useful strategies for doing this.

The most commonly used "metric" of the past for demonstrating the realism of climate models is the global

warming that has occurred over the twentieth century. Older generations of climate GCMs generally matched the twentieth century warming quite well. However, *Kiehl* (2007) showed that they did this despite a wide variety of climate forcings and climate sensitivities (within the observational uncertainties) because the forcings and sensitivities were negatively correlated. For example, a model with more aerosol cooling might also have a higher sensitivity to CO_2. The current CMIP5 generation of models does not show this behavior (*Forster et al.,* 2013) (Fig. 13), although a subset of the models that agrees best with the observed temperature trend does, perhaps because most current models now try to include the very uncertain aerosol indirect effect on clouds. This causes some models to depart from the observed trend to an extent not seen in older models. Observations are not yet good enough to tell us the correct combination of forcing and feedback, hence we cannot use the twentieth century temperature record to "validate" climate models. On the other hand, no GCM with only natural climate forcings has ever been able to reproduce the observed warming; this is perhaps the best evidence we have that the warming of recent decades is due to anthropogenic influences (*Knutti,* 2008). In this sense today's climate models are "wrong but useful" (*Schmidt,* 2009).

A caveat to the statements above is the chaotic nature of the climate system. Weather forecasts are sensitive to errors in the initial conditions and the parameterization of unresolved processes such as moist convection and thus must be considered probabilistic (*Slingo and Palmer,* 2011). One can then ask to what extent long-term climate change is predictable. *Lorenz* (1968) considered a possible "almost intransitive" climate system whose statistics were insensitive to initial conditions on infinite timescales but sensitive to initial conditions over long but finite time intervals. *Hasselmann* (1976) showed how short-term weather acts as a stochastic forcing whose effect is integrated by slow components of the climate system (e.g., the upper ocean) to produce longer timescale variations in sea surface temperatures. The twentieth century climate appears to have unforced decadal variations, perhaps due to episodes of deep ocean heat storage (and little surface warming) alternating with episodes of greater near-surface warming. To date, however, ensemble climate model integrations over many centuries do not exhibit the longer-term, larger-amplitude natural variability required for the twentieth century to be explained as the behavior of an almost intransitive system. Uncertainty in future climate projections is dominated instead by uncertainty in model physics (*Slingo and Palmer,* 2011), as we discuss next.

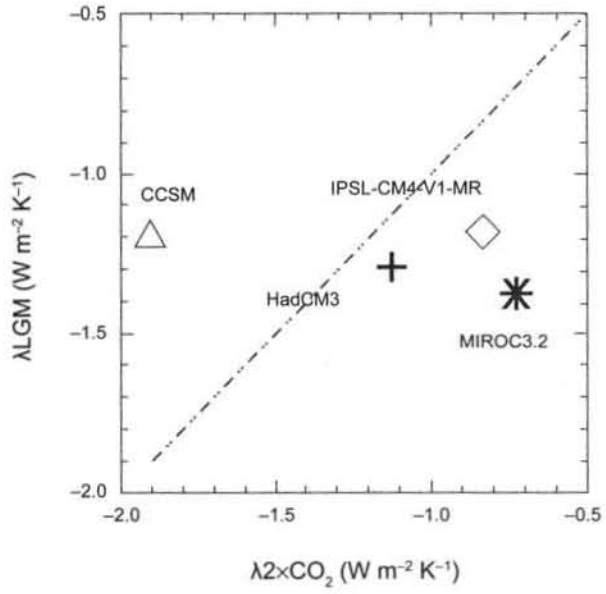

Fig. 12. The climate sensitivity parameter λ simulated by four GCMs for the LGM vs. the same sensitivity parameter of each model for $2\times CO_2$. In equilibrium the sensitivity parameter $\lambda = \Delta T_s/G$, where G is the external radiative forcing applied and ΔT_s is the equilibrium surface temperature response to the forcing. If the sensitivity parameter were identical to LGM and $2\times CO_2$ forcing for each GCM, the points would lie along the 45° (dash-double dot) line. From *Crucifix* (2006). ©Copyright American Geophysical Union; reprinted with permission.

4.2. How Well Can We Project Future Climate Warming?

Climate GCMs have been used to project future climate change for four decades, but the uncertainty in the $2CO_2$ ΔT_s has not changed much. A doubling of CO_2 concentration by itself warms the surface temperature by ~1.2°C, yet for much of the history of climate modeling, the $2\times CO_2$ ΔT_s of different climate models has ranged from ~1.5° to 4.5°C. The reason for the difference is feedbacks that either amplify (positive feedback) or mitigate (negative feedback) the original CO_2-forced climate change (see Covey et al., this volume, for a detailed discussion). Briefly, the primary feedbacks and their sign are the Planck feedback due to increased emission to space from a warmer atmosphere (negative); the water vapor feedback due to the greenhouse effect of the water vapor added by evaporation from a warmer surface (positive); the lapse rate feedback due primarily to the temperature dependence of the moist adiabatic lapse rate, which increases warming at altitude at the expense of that at the surface (negative); the snow/ice-albedo feedback from the decrease in planetary albedo caused by melting snow and sea ice as climate warms (positive); and the cloud feedback due to changes in cloud cover, height, and optical thickness.

Quantitative differences exist among models in the Planck, water vapor, lapse rate, and snow/ice-albedo feedbacks (Fig. 14), but their sign is not in doubt. Most of the spread in ΔT_s comes from uncertainty in the sign and magnitude of the cloud feedback. It is often claimed that as climate warms, more water evaporates from the oceans, making more cloud, which reflects more sunlight, a negative feedback. But clouds do not depend on the mixing ratio of water

vapor (which changes dramatically with temperature, given the Clausius-Clapeyron equation) but rather the relative humidity (the mixing ratio relative to its saturation value), static stability, and other environmental factors, which do not obviously vary with warming in a direction that would either increase or decrease cloud. Furthermore, clouds at different altitudes have radiative effects of opposite sign. Low stratocumulus clouds, which reflect considerable sunlight but have little effect on outgoing LW radiation (Fig. 3), cool the planet, so increasing/decreasing them would be a negative/positive feedback. Cirrus clouds, on the other hand, are thinner and reflect less sunlight, but lie above the clear sky emission to space level and thus reduce LW emission to space, so increasing/decreasing them would be a positive/negative feedback. Changes in cloud height and optical thickness contribute to the cloud feedback as well, more so for some cloud types in some places than others. This makes representing cloud effects in one-dimensional models of exoplanet habitable zones (*Kitzman et al.,* 2010; *Zsom et al.,* 2012) a tremendous challenge.

For the CMIP3 generation of climate models, cloud feedback as evaluated by the climate change in cloud forcing varied from negative to near-neutral to positive, according to *Soden et al.* (2008) (Fig. 14), consistent with the canonical wisdom that we do not know the sign of cloud feedback. *Soden and Held* (2006), however, note that the cloud forcing method of calculating feedback is biased because the cloud effect on radiation is differenced against the clear sky radiative fluxes, which also change as the climate changes. By calculating "radiative kernels" that represent the partial derivatives of TOA fluxes with respect to different feedback parameters, they derive an adjusted cloud forcing change that is a more accurate depiction of the cloud feedback. Determined in this way, all the CMIP3 models have either a near-neutral or positive cloud feedback (Fig. 14), the opposite of the canonical wisdom. Furthermore, the range of CMIP3 climate sensitivities is 2.1°–4.4°C, i.e., the lowest sensitivities are no longer being simulated by any model.

Early indications from the current CMIP5 GCMs are that the situation has not changed dramatically, but now the sources of the net positive cloud feedback are being understood (*Zelinka et al.,* 2013): a positive LW cloud feedback due to an upward shift in the altitude of high clouds, and a positive SW feedback due to a decrease in total cloudiness outside the polar regions. The former is a robust consequence of the deepening of convection as the surface warms. The latter is a combination of two effects: a poleward shift of the storm tracks as the Hadley cell expands, also a robust result, and a decrease in low-latitude stratocumulus and shallow cumulus cloud cover, which may be understood (*Brient and Bony,* 2012) but is not thought to be reliably simulated by GCMs with coarse vertical resolution. At high latitudes, cloud optical thickness tends to increase with warming, a negative feedback. The response of climate model clouds to warming can be summarized as an "upward and outward" shift of clouds from the tropical lower troposphere to higher

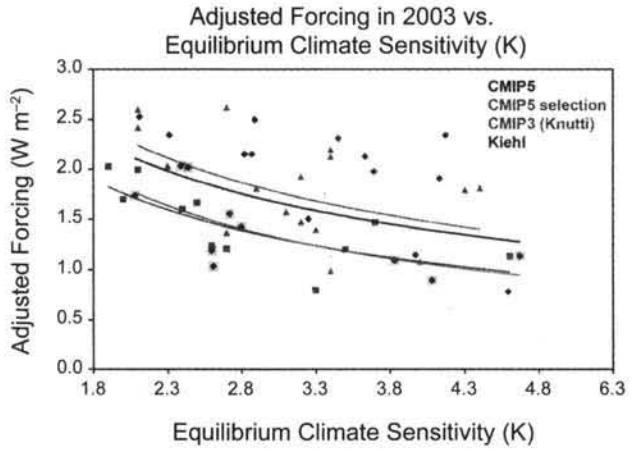

Fig. 13. See Plate 6 for color version. The relationship between 2003 climate forcing and equilibrium climate sensitivity for the turn-of-century GCMs analyzed by *Kiehl* (2007) (red), the CMIP3 GCMs analyzed by *Knutti* (2008) (blue), the CMIP5 GCMs (black), and a subset of CMIP5 GCMs that are within the 90% uncertainty range of the observed 100-year linear temperature trend (green). From *Forster et al.* (2013). ©Copyright American Geophysical Union; reprinted with permission.

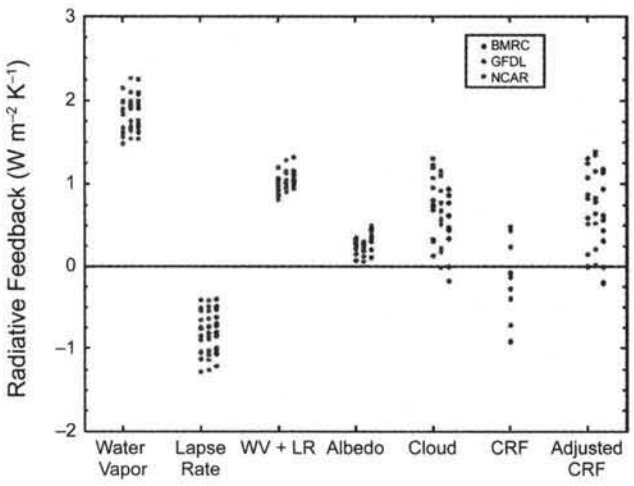

Fig. 14. Radiative feedbacks in response to $2\times CO_2$ for a large selection of GCMs. The symbols in a given column portray the range of feedbacks over all the models. The three different columns represent the same feedbacks calculated using radiative kernels obtained from three different GCMs as the baseline. The first five columns show the water vapor, lapse rate, combined water vapor + lapse rate, surface albedo (primarily snow/ice), and cloud feedbacks. The sixth column shows cloud feedback calculated using the traditional method of the change in cloud forcing, and the seventh column shows the results for an adjusted cloud forcing method that takes account of clear sky changes. From *Soden et al.* (2008). ©Copyright 2008 American Meteorological Society; reprinted with permission.

altitudes and latitudes (*Zelinka et al.,* 2013).

The CMIP5 models are an "ensemble of opportunity," i.e., a sample of the models that happen to exist today with "structural" differences (resolution, parameterization approaches) but that do not represent the full range of feedback uncertainty. A different approach is the "perturbed parameter ensemble," a set of thousands of simulations using a single climate model but with free parameters altered from one simulation to the next over the range of their uncertainty. This produces a probability density function of climate sensitivity whose 5–95% range of probability is not very different from that of the ensemble of opportunity except for some probability of climate sensitivities much greater than any ever simulated by an operational model (*Stainforth et al.,* 2005). With the perturbed parameter approach one can identify which parameters have the greatest effect on the model's sensitivity. Analysis of this ensemble suggests that ΔT_s (in the context of one particular GCM) is most sensitive to assumptions about the rate of entrainment of dry air into convective updrafts, the fall speed of ice crystals, and parameters that affect the formation of clouds and precipitation (*Sanderson et al.,* 2010).

The climate sensitivities simulated by today's GCMs incorporate only "fast" feedbacks due to atmospheric or near-surface processes. On longer timescales, "slow" feedbacks due to continental ice sheet growth and retreat, vegetation changes, and carbon fluxes into and out of the atmosphere, soil, biosphere, and ocean can produce an "Earth system sensitivity" quite different from the climate sensitivity due to fast feedbacks. Estimates of this sensitivity suggest that it could be 50–100% larger than the ~3°C median fast feedback sensitivity (*Lunt et al.,* 2010; *Park and Royer,* 2011). Furthermore, even for the fast feedbacks, climate sensitivity is expected to depend on atmospheric state. Thus it may vary from that portrayed by the CMIP5 models when larger climate excursions are considered and thresholds for qualitatively different behaviors of climate system components are crossed (*Hansen et al.,* 2013).

The apparent preponderance of positive feedbacks in the Earth system thus makes continued future warming highly probable. Furthermore, with the caveat that exoplanet science considers variations much larger and nonlinear than those discussed here, what we know about Earth also may have implications for assessments of the habitable zone of Earth-like planets:

1. Ocean heat transport, which retards the sea ice growth (Fig. 7) and tropical/polar heating imbalance that helps determine habitable zone limits, but which is missing from most exoplanet models (e.g., *Abe et al.* 2011), may broaden the habitable zone.

2. The negative net cloud forcing of Earth's climate (Fig. 3) may shift the habitable zone inward relative to estimates that use a cloud-free atmosphere (*Kopparapu et al.,* 2013).

3. The likelihood that many fast and slow feedbacks on Earth are positive offsets some part of the ocean- and cloud-forcing impacts, and would shrink the habitable zone.

5. CONCLUSIONS

Much remains to be better understood about Earth's climate: how convection interacts with the general circulation in different dynamic and thermodynamic environments; how aerosols, radiation, and clouds interact with turbulence to determine the presence or absence of marine stratocumulus clouds; how stratospheric circulations affect the troposphere; how stable continental ice sheets are to perturbations; and so on. Even when we understand the basic physics, we are not yet able to always portray it properly in GCMs that do not resolve the processes, and this limits our predictive ability.

Nonetheless, our accumulated knowledge about Earth can serve as a valuable resource for solar system and exoplanet atmospheric scientists. For exoplanets, inferences are limited by our inability to resolve spatial details of observed planets. Thus, one might observe Earth remotely as if it were an exoplanet (*Karalidi et al.,* 2012), not to learn anything new about Earth, but to use our detailed knowledge of its spatially varying radiative properties to understand how best to interpret a disk-integrated exoplanet spectrum. Likewise, a chronic sampling problem plagues solar system science because missions visit specific planets only occasionally and often do not monitor them globally and continuously. Is the composition and thermodynamic structure observed by a single planetary probe typical of the global mean? Do differences between snapshots of a planet taken by a past flyby and a current orbiter indicate a climate change or random samples of natural variability? Our sparse observations of other planets might be placed into an appropriate context by sampling Earth satellite datasets or reanalyses in a similar way and asking how representative those samples are of conditions elsewhere or at other times.

More importantly, our understanding of the mechanisms that conspire to produce Earth's weather and climate should probably be used as the starting point for trying to interpret any new observation of another planet. Often Earth is a valuable guide to the physics operating on other terrestrial planets: baroclinic waves on Mars, deep moist convection on Titan, photochemical sulfuric acid aerosols on Venus. When this is not the case, asking why not brings deeper insights than considering either planet in isolation. The same applies in the opposite direction: The terrestrial atmospheric community would benefit greatly from thinking more often about other planets and testing the depth of their understanding by bringing it to a different part of parameter space. Such a planetary perspective on our own planet will help us identify the fundamental unanswered questions that will advance the science the furthest.

REFERENCES

Abbot D. S., Voigt A., Branson M., Pierrehumbert R. T., Pollard D., Le Hir G., and Koll D. D. B. (2012) Clouds and snowball Earth deglaciation. *Geophys. Res. Lett., 39,* L20711, DOI: 10.1029/2012GL052861.

Abe Y., Abe-Ouchi A., Sleep N. H., and Zahnle K. J. (2011) Hab-

itable zone limits for dry planets. *Astrobiology, 11,* 443–460.

Allison M., Del Genio A. D., and Zhou W. (1995) Richardson number constraints for the Jupiter and outer planet wind regime. *Geophys. Res. Lett., 22,* 2957–2960.

Bauer S. E., Wright D., Koch D., Lewis E. R., McGraw R., Chang L.-S., Schwartz S. E., and Ruedy R. (2008) MATRIX (Multiconfiguration Aerosol TRacker of mIXing state): An aerosol microphysical module for global atmospheric models. *Atmos. Chem. Phys.*, 8, 6003–6035.

Brady E. C., Otto-Bliesner B. L., Kay J. E., and Rosenbloom N. (2013) Sensitivity to glacial forcing in the CCSM4. *J. Climate, 26,* 1901–1925.

Brient F. and Bony S. (2012) Interpretation of the positive low-cloud feedback predicted by a climate model under global warming. *Climate Dynam., 40,* 2415–2431, DOI: 10.1007/s00382-011-1279-7.

Broecker W. S. (1991) The great ocean conveyor. *Oceanography, 4,* 79–89.

Collins M., Booth B. B. B., Bhaskaran B., Harris G. R., Murphy J. M., Sexton D. M. H., and Webb M. J. (2011) Climate model errors, feedbacks and forcings: A comparison of perturbed-physics and multi-model ensembles. *Climate Dynam., 36,* 1737–1766.

Conrath B. J. and Pirraglia J. A. (1983) Thermal structure of Saturn from Voyager infrared measurements: Implications for atmospheric dynamics. *Icarus, 53,* 286–292.

Costa S. M. S. and Shine K. P. (2012) Outgoing longwave radiation due to directly transmitted surface emission. *J. Atmos. Sci., 69,* 1865–1870.

Crucifix M. (2006) Does the last glacial maximum constrain climate sensitivity? *Geophys. Res. Lett., 33,* L18701, DOI: 10/1029/2006GL027137.

Del Genio A. D. (2012) Representing the sensitivity of convective cloud systems to tropospheric humidity in general circulation models. *Surv. Geophys., 33,* 637–656.

Del Genio A. D., Zhou W., and Eichler T. P. (1993) Equatorial superrotation in a slowly rotating GCM: Implications for Titan and Venus. *Icarus, 101,* 1–17.

Enderton D. and Marshall J. (2009) Explorations of atmosphere-ocean-ice climates on an aquaplanet and their meridional energy transports. *J. Atmos. Sci., 66,* 1593–1611.

Ferreira D., Marshall J., and Rose B. (2011) Climate determinism revisited: Multiple equilibria in a complex climate model. *J. Climate, 24,* 992–1012.

Forster P. M., Andrews T., Good P., Gregory J. M., Jackson L. S., and Zelinka M. (2013) Evaluating adjusted forcing and model spread for historical and future scenarios in the CMIP5 generation of climate models. *J. Geophys. Res.–Atmos., 118,* 1–12.

Frierson D. M. W. (2008) Midlatitude static stability in simple and comprehensive general circulation models. *J. Atmos. Sci., 65,* 1049–1062.

Gierasch P. J. (1976) Jovian meteorology: Large-scale moist convection. *Icarus, 29,* 445–454.

Hansen J., Lacis A., Rind D., Russell G., Stone P., Fung I., Ruedy R., and Lerner J. (1984) Climate sensitivity: Analysis of feedback mechanisms. In *Climate Processes and Climate Sensitivity* (J. E. Hansen and T. Takahashi, eds.), pp. 130–163. AGU Geophys. Monogr. 29, Maurice Ewing Vol. 5, American Geophysical Union, Washington, DC.

Hansen J., Russell G., Lacis A., Fung I., Rind D., and Stone P. (1985) Climate response times: Dependence on climate sensitivity and ocean mixing. *Science, 229,* 857–859.

Hansen J., Sato M., Ruedy R., et al. (2005) Efficacy of climate forcings. *J. Geophys. Res., 110,* D18104, DOI: 10.1029/2005JD005776.

Hansen J., Sato M., Russell G., and Kharecha P. (2013) Climate sensitivity, sea level, and atmospheric CO_2. *Philos. Trans. R. Soc. A,* in press, arXiv: 1211.4846v2.

Hargreaves J. C. and Annan J. D. (2009) On the importance of paleoclimate modeling for improving predictions of future climate change. *Climate Past, 5,* 803–814.

Hargreaves J. C., Annan J. D., Yoshimori M., and Abe-Ouchi A. (2012) Can the Last Glacial Maximum constrain climate sensitivity? *Geophys. Res. Lett., 39,* L24702, DOI: 10.1029/2012GL053872.

Hasselmann K. (1976) Stochastic climate models. *Tellus, 28,* 473–485.

Houghton J. T. (2002) *The Physics of Atmospheres, 3rd edition.* Cambridge Univ., Cambridge. 340 pp.

Jones T. R. and Randall D. A. (2011) Quantifying the limits of convective parameterizations. *J. Geophys. Res., 116,* D08210, DOI: 10.1029/2010JD014913.

Karalidi T., Stam D. M., Snik F., Bagnulo S., Sparks W. B., and Keller C. U. (2012) Observing the Earth as an exoplanet with LOUPE, the lunar observatory for unresolved polarimetry of Earth. *Planet. Space Sci., 74,* 202–207.

Kiehl J.T. (2007) 20th century climate model response and climate sensitivity. *Geophys. Res. Lett., 34,* L22710.

Kitzman D., Patzer A. B. C., von Paris P., Godolt M., Stracke B., Gebauer S., Grenfell J. L., and Rauer H. (2010) Clouds in the atmospheres of extrasolar planets. 1. Climatic effects of multi-layer clouds for Earth-like planets and implications for habitable zones. *Astron. Astrophys., 511,* A66.

Klinger B. A. and Marotzke J. (2000) Meridional heat transport by the subtropical cell. *J. Phys. Ocean., 30,* 696–705.

Klocke D., Pincus R., and Quaas J. (2011) On constraining estimates of climate sensitivity with present-day observations through model weighting. *J. Climate, 24,* 6092–6099.

Knutti R. (2008) Why are global climate models reproducing the observed global surface warming so well? *Geophys. Res. Lett.*, 35, L18704, DOI: 10.1029/2008GL034932.

Koch D. and Del Genio A. D. (2010) Black carbon semi-direct effects on cloud cover: Review and synthesis. *Atmos. Chem. Phys., 10,* 7685–7696.

Kopp G. and Lean J. L. (2011) A new, lower value of total solar irradiance: Evidence and climate significance. *Geophys. Res. Lett., 38,* L01706, DOI: 10.1029/2010GL045777.

Kopparapu R. K., Ramirez R., Kasting J. F., Eymet V., Robinson T. D., Mahadevan S., Terrien R., Domagal-Goldman S., Meadows V., and Deshpande R. (2013) Habitable zones around main-sequence stars: New estimates. *Astrophys. J., 765,* A131.

Lacis A. A., Schmidt G. A., Rind D., and Ruedy R. A. (2010) Atmospheric CO_2: Principal control knob governing Earth's temperature. *Science, 330,* 356–359.

Loeb N. G., Wielicki B. A., Doelling D. R., Smith G. L., Keyes D. F., Kato S., Manalo-Smith N., and Wong T. (2009) Toward optimal closure of the Earth's top-of-atmosphere radiation budget. *J. Climate, 22,* 748–766.

Lorenz E. L. (1968) Climatic determinism. *Meteorol. Monogr. Am. Meteorol. Soc., 25,* 1–3.

Lunt D. J., Haywood A. M., Schmidt G. A., Salzmann U., Valdes P. J., and Dowsett H. J. (2010) Earth system sensitivity inferred from Pliocene modeling and data. *Nature Geosci., 3,* 60–64.

Lyman J. M., Good S. A., Gouretski V. V., Ishii M., Johnson G. C.,

Palmer M. D., Smith D. M., and Willis J. K. (2010) Robust warming of the global upper ocean. *Nature, 465,* 334–337.

Manabe S. and Strickler R. F. (1964) Thermal equilibrium of the atmosphere with a convective adjustment. *J. Atmos. Sci., 21,* 361–385.

McComiskey A. and Feingold G. (2012) The scale problem in quantifying aerosol indirect effects. *Atmos. Chem. Phys., 12,* 1031–1049.

McKay C. P., Pollack J. B., and Courtin R. (1991) The greenhouse and antigreenhouse effects on Titan. *Science, 253,* 1118–1121.

McKay C. P., Lorenz R. D., and Lunine J. I. (1999) Analytic solutions for the antigreenhouse effect: Titan and the early Earth. *Icarus, 137,* 56–61.

Mitchell J. L. (2012) Titan's transport-driven methane cycle. *Astrophys. J. Lett., 756,* L26.

Myhre G. (2009) Consistency between satellite-derived and modeled estimates of the direct aerosol effect. *Science, 325,* 187–190.

O'Gorman P. A. (2011) The effective static stability experienced by eddies in a moist atmosphere. *J. Atmos. Sci.*, 68, 75–90.

Park J. and Royer D. L. (2011) Geologic constraints on the glacial amplification of Phanerozoic climate sensitivity. *Am. J. Sci., 311,* 1–26.

Pincus R., Batstone C. P., Hofmann R. P. J., Taylor K. E., and Gleckler P. J. (2008) Evaluating the present-day simulation of clouds, precipitation, and radiation in climate models. *J. Geophys. Res., 113,* D14209, DOI: 10.1029/2007JD009334.

Poulsen C. and Jacob R. (2004) Factors that inhibit snowball Earth simulation. *Paleoceanography, 19,* PA4021, DOI: 10.1029/2004PA001056.

Reichler T. and Kim J. (2008) How well do coupled models simulate today's climate? *Bull. Am. Meteorol. Soc., 89,* 303–311.

Rind D. (2008) The consequences of not knowing low- and high-latitude climate sensitivity. *Bull. Am. Meteorol. Soc., 89,* 855–864.

Rose B. E. J. and Marshall J. (2009) Ocean sea ice, heat transport, and multiple climate states: Insights from energy balance models. *J. Atmos. Sci., 66,* 2828–2843.

Sanderson B. M., Shell K. M., and Ingram W. (2010) Climate feedbacks determined using radiative kernels in a multi-thousand member ensemble of AOGCMs. *Climate Dynam., 30,* 175–190.

Schmidt G. (2009) Wrong but useful. *Phys. World, 13,* 33–35.

Schmidt G. A., Ruedy R., Miller R. L., and Lacis A. A. (2010) The attribution of the present-day total greenhouse effect. *J. Geophys. Res., 115,* D20106, DOI: 10.1029/2010JD014287.

Schmidt G. A., Annan J. D., Bartlein P. J., Cook B. I., Guilyardi E., Hargreaves J. C., Harrison S. P., Kageyama M., LeGrande A. N., Konecky B., Lovejoy S., Mann M. E., Masson-Delmotte V., Risi C., Thompson D., Timmermann A., Tremblay L.-B., and Yiou P. (2013) Using paleo-climate comparisons to constrain future projections in CMIP5. *Climate Past,* in press, DOI: 10.5194/cpd-9-775-2013.

Slingo J. and Palmer T. (2011) Uncertainty in weather and climate prediction. *Philos. Trans. R. Soc. A, 369,* 4751–4767.

Soden B. J. and Held I. M. (2006) An assessment of climate feedbacks in coupled ocean-atmosphere models. *J. Climate, 19,* 3354–3360.

Soden B. J., Held I. M., Colman R., Shell K. M., Kiehl J. T., and Shields C. A. (2008) Quantifying climate feedbacks using radiative kernels. *J. Climate, 21,* 3504–3520.

Sohl L. E. and Chandler M. A. (2007) Reconstructing Neoproterozoic palaeoclimates using a combined data/modelling approach. In *Deep-Time Perspectives on Climate Change: Marrying the Signal from Computer Models and Biological Proxies* (M. Williams et al., eds.), pp. 61–80. Micropalaeontological Society Spec. Publ. #2.

Stainforth D. A., Aina T., Christensen C., Collins M., Faull N., Frame D. J., Kettleborough J. A., Knight S., Martin A., Murphy J. M., Piani C., Sexton D., Smith L. A., Spicer R. A., Thorpe A. J., and Allen M. R. (2005) Uncertainty in predictions of the climate response to rising levels of greenhouse gases. *Nature, 433,* 403–406.

Stephens G. L., Li J., Wild M., Clayson C. A., Loeb N., Kato S., L'Ecuyer T., Stackhouse P. W. Jr., Lebsock M., and Andrews T. (2012) An update on Earth's energy balance in light of the latest global observations. *Nature Geosci., 5,* 691–696.

Stone P. H. (1978a) Constraints on dynamical transports of energy on a spherical planet. *Dynam. Atmos. Oceans, 2,* 123–139.

Stone P. H. (1978b) Baroclinic adjustment. *J. Atmos. Sci., 35,* 561–571.

Strobel D. F., Atreya S. K., Bézard B., Ferri F., Flasar F. M., Fulchignoni M., Lellouch E., and Muller-Wodarg I. (2009) Atmospheric structure and composition. In *Titan from Cassini-Huygens* (R. H. Brown et al., eds.), Chapter 10, pp. 235–257, DOI: 10.1007/978-1-4020-9215-2_10. Springer Dordrecht, Heidelberg-London-New York.

Trenberth K. E. and Caron J. M. (2001) Estimates of meridional atmosphere and ocean heat transports. *J. Climate, 14,* 3433–3443.

Trenberth K. E., Smith L., Qian T., Dai A., and Fasullo J. (2007) Estimates of the global water budget and its annual cycle using observational and model data. *J. Hydrometeor., 8,* 758–769.

Turtle E. P., Del Genio A. D., Barbara J. M., Perry J. E., Schaller E. L., McEwen A. S., West R. A., and Ray T. L. (2011) Seasonal changes in Titan's meteorology. *Geophys. Res. Lett., 38,* L03203, DOI: 10.1029/2010GL046266.

Waelbroeck C. and MARGO Project Members (2009) Constraints on the magnitude and patterns of ocean cooling at the Last Glacial Maximum. *Nature Geosci., 2,* 127–132.

Wallace J. M. and Hobbs P. V. (2006) *Atmospheric Science: An Introductory Survey, 2nd edition.* Academic, New York. 504 pp.

Ye B., Del Genio A. D., and Lo K. K.-W. (1998) CAPE variations in the current climate and in a climate change. *J. Climate, 11,* 1997–2015.

Zelinka M. D. and Hartmann D. L. (2011) The observed sensitivity of high clouds to mean surface temperature anomalies in the tropics. *J. Geophys. Res., 116,* D23103, DOI: 10.1029/2011JD016459.

Zelinka M. D., Klein S. A., Taylor K. E., Andrews T., Webb M. J., Gregory J. M., and Forster P. M. (2013) Contributions of different cloud types to feedbacks and rapid adjustments in CMIP5. *J. Climate,* in press, DOI: 10.1175/JCLI-D-12-00555.1.

Zimmer M., Craig G. C., Keil C., and Wernli H. (2011) Classification of precipitation events with a convective response timescale and their forcing characteristics. *Geophys. Res. Lett., 38,* L05802, DOI: 10.1029/2010GL046199.

Zipser E. J. and Lutz K. R. (1994) The vertical profile of radar reflectivity of convective cells: A strong indicator of storm intensity and lightning probability? *Mon. Weather Rev., 122,* 1751–1759.

Zsom A., Kaltenegger L., and Goldblatt C. (2012) A 1D microphysical cloud model for Earth, and Earth-like exoplanets: Liquid water and water ice clouds in the convective troposphere. *Icarus, 221,* 603–616.